dipole-dipole interactions between highly excited Rydberg atoms [6], cavity-mediated photon exchange [7] and controlled ground-state collisions [8]. These quantum systems have been employed to demonstrate a two-qubit controlled-NOT gate [9] and the entanglement of two individual atoms [10]. Decoherence represents a loss of information and can be a serious limitation. Therefore coherence times need be considerably longer than initialization, multiqubit interaction and measurement times. Especially for scaling to plenty of atoms in the optical lattice, long coherence time is crucial to the storage and the manipulation of quantum information. For precision metrology, an interferometer consisting of only one atom is suitable to investigate the localized forces near surface [11, 12]. However, in the interferometer the effect of increasing sensitivity competes with the decreased ratio of signal to noise. Suppressing decoherence leads to prolongation of the measurement time while keeping large signal, and thus improves the precision.

Quantum decoherence is due to coupling between quantum system and its surrounding environment, including the longitudinal spin relaxation (T_1) and the transverse phase relaxation (T_2). In a far-off-resonance trap (FORT), the spin relaxation of atoms is due to the spontaneous Raman scattering of photons from the trap laser [13]. A spin relaxation time of several seconds is achieved, owing to the large detuning. Therefore, a key issue is the improvement in phase coherence. As described in [14], it is important to distinguish between inhomogeneous and homogeneous processes. Inhomogeneous dephasing (T_2^*) originates from the energy distribution of trapped atoms which results in a distribution of light shift. In comparison with reversible inhomogeneous process, the homogeneous dephasing (T_2') affects each atom in the same way and cannot be reversed. Common mechanisms are the dipole trap laser intensity fluctuations, beam pointing instability, magnetic field fluctuations and heating of atoms. In order to suppress phase decoherence, a plenty of multipulse dynamical decoupling techniques are investigated, such as the Carr-Purcell-Meiboom-Gill (CPMG), Uhrig dynamical decoupling (UDD), concatenated dynamical decoupling (CDD) and periodic dynamical decoupling (PDD). One of these, the CPMG pulse sequence is derived from spin echo and widely used in the field of nuclear magnetic resonance [15]. Recently, multipulse sequences have been applied to improve phase coherence of qubits in a variety of systems, including semiconductor quantum dots [16], solid state superconductor [17], nitrogen-vacancy centers in diamond [18], electron paramagnetic resonance in molecules [19], polarisation states of photons [20, 21], atomic and ionic ensembles [22–24], and single ions [25].

In this paper we investigate coherence of single ^{87}Rb atoms in an optical dipole trap and strongly suppress dephasing utilizing CPMG pulse sequence. Though the spin echo technique was applied for single atoms [14, 26–28], CPMG sequence was not studied until the theoretical investigation of multipulse sequences in [29]. The authors examined the performance of variety of pulse sequences and found that CPMG pulse sequence was an excellent choice for suppressing both inhomogeneous and homogeneous dephasing mechanisms. To date, experimental demonstration of its effect remains unexplored. Here we extend CPMG sequence to single neutral atoms and successfully observe the strong suppression effect. For our trap $U_0 = 0.7$ mK, the spin relaxation time is $T_1 = 0.83 \pm 0.11$ s. We obtain the inhomogeneous dephasing time of $T_2^* = 1.4 \pm 0.1$ ms. Utilizing CPMG sequence with pulse number $n = 6$, the homogeneous dephasing time is extended to $T_2' = 304 \pm 17$ ms. It is prolonged by a factor of 3 in comparison with the result of spin echo.

2. Theoretical analysis of CPMG sequence

The CPMG pulse sequence is regarded as repetition of spin echo. It is composed of n π-pulses (at times $t_k = (2k-1)\tau, k = 1, 2, \ldots, n$, where τ is the time of the first π-pulse) between two $\pi/2$-pulses at times 0 and t. Time t can be varied to map out the corresponding fringes. Via

#200990 - $15.00 USD Received 7 Nov 2013; revised 5 Dec 2013; accepted 9 Dec 2013; published 18 Dec 2013

CPMG pulse sequence, the inhomogeneous dephasing is reversed, and the homogeneous dephasing also be successfully suppressed.

We refer to the analytical model presented in [14] to account for the inhomogenous dephasing of CPMG sequence. Single atoms are localized in a harmonic optical dipole trap. The hyperfine structure levels of ground state experience different light shifts. Resulting from the energy distribution of trapped atoms, a distribution of differential light shift $\delta_{\rm ls}$ is given by [14]

$$p(\delta_{\rm ls}) = \frac{1}{2k_BT}\left(\frac{2\hbar\Delta_{\rm eff}}{k_BT\,\omega_{\rm hfs}}\right)^2(\delta_{\rm ls}-\delta_0)^2\exp\left[-\frac{2\hbar\Delta_{\rm eff}}{k_BT\,\omega_{\rm hfs}}(\delta_{\rm ls}-\delta_0)\right], \tag{1}$$

where δ_0 is the maximum differential light shift, $\omega_{\rm hfs}$ is the ground state hyperfine splitting, and $\Delta_{\rm eff}$ is an effective detuning, including the effects of the D_1 and D_2 transitions. Using the Bloch vector formalism, we define the matrices:

$$\mathbf{\Phi}_{\pi/2} = \begin{pmatrix} 1 & 0 & 0 \\ 0 & 0 & -1 \\ 0 & -1 & 0 \end{pmatrix}, \tag{2}$$

$$\mathbf{\Phi}_{\pi} = \begin{pmatrix} 1 & 0 & 0 \\ 0 & -1 & 0 \\ 0 & 0 & -1 \end{pmatrix}, \tag{3}$$

$$\mathbf{\Psi}_{\rm free}(\delta,t) = \begin{pmatrix} \cos(\delta t) & \sin(\delta t) & 0 \\ -\sin(\delta t) & \cos(\delta t) & 0 \\ 0 & 0 & 1 \end{pmatrix}. \tag{4}$$

They describe the action of $\pi/2$-pulse and π-pulse, the free precession with frequency δ, respectively.

The initial state corresponds to the Bloch vector $\mathbf{U}_0 \equiv (u,v,w) = (0,0,-1)$. After applying CPMG sequence, the Bloch vector evolves as

$$\begin{aligned} \boldsymbol{U}_{\rm CPMG}(t) = {} & \mathbf{\Phi}_{\pi/2}\times\mathbf{\Psi}_{\rm free}(\delta,t-(2n-1)\tau)\times\mathbf{\Phi}_{\pi} \\ & \times\underbrace{\mathbf{\Psi}_{\rm free}(\delta,2\tau)\times\mathbf{\Phi}_{\pi}\times\cdots\times\mathbf{\Psi}_{\rm free}(\delta,2\tau)\times\mathbf{\Phi}_{\pi}}_{n-1\text{ groups}}\times\mathbf{\Psi}_{\rm free}(\delta,\tau)\times\mathbf{\Phi}_{\pi/2}\times\boldsymbol{U}_0. \end{aligned} \tag{5}$$

From this equation, we obtain the third component of the Bloch vector, w,

$$w_{\rm CPMG}(t) = (-1)^n\cos\left[\delta(t-2n\tau)\right]. \tag{6}$$

The shape of the CPMG fringe is calculated by integrating,

$$\begin{aligned} w_{\rm CPMG,inh}(t) &= (-1)^n\int_0^\infty p(\delta_{ls})\cos\left[(\delta_{\rm set}-\delta_{\rm B}-\delta_{\rm ls})\,(t-2n\tau)\right]d\delta_{\rm ls} \\ &= (-1)^n\alpha\,(t-2n\tau,T_2^*)\cos\left[\delta'(t-2n\tau)+\kappa\,(t-2n\tau,T_2^*)\right], \end{aligned} \tag{7}$$

with

$$\alpha\,(t-2n\tau,T_2^*) = \left[1+0.95(t-2n\tau)^2/T_2^{*2}\right]^{-3/2}, \tag{8}$$

$$\kappa\,(t-2n\tau,T_2^*) = -3\arctan\left[0.97(t-2n\tau)/T_2^*\right], \tag{9}$$

where $\delta_{\rm set} = \omega-\omega_{\rm hfs}$ is the detuning, $\delta_{\rm B}$ is the quadratic Zeeman shift,and $\delta' = \delta_{\rm set}-\delta_{\rm B}-\delta_{\rm ls}$ represents the sum of the detunings. The inhomogenous dephasing time T_2^* is defined as the $1/e$ time of the amplitude α.

#200990 - $15.00 USD Received 7 Nov 2013; revised 5 Dec 2013; accepted 9 Dec 2013; published 18 Dec 2013

In order to reveal the effects of suppressing homogenous dephasing, we fit the visibility signals of CPMG sequences with a Gaussian,

$$V(t) = C_0 \exp\left[-\left(\frac{t}{T_2'}\right)^2\right]. \tag{10}$$

Here, T_2' is the homogenous dephasing time.

3. Experimental tools and results

3.1. Experimental setup

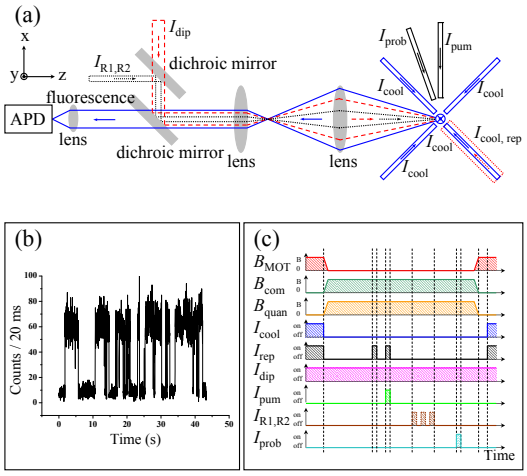

Fig. 1. (a) Schematic of experimental setup. The quantization axis is defined by a magnetic field along the z-axis. The ^{87}Rb MOT is formed by six cooling lasers (I_{cool}) and an overlap repumping laser (I_{rep}). A laser beam with 830 nm wavelength (I_{dip}) is tightly focused to a waist of 2.1 μm. The resulting optical potential depth is 0.7 mK for a laser power of 7 mW. The fluorescence of single atoms is detected with an avalanche photodiode. The initial state is prepared using an optical pumping laser beam (I_{pum}) in combination with the repumping beam. The Raman laser beams ($I_{\mathrm{R1}}, I_{\mathrm{R2}}$) at 795 nm are coupled into the same polarization maintaining optical fiber and focused onto single atoms. For the state-selective detection, a probe laser beam (I_{prob}) is applied. (b) Measured fluorescence signals of single atoms within 20 ms time bins. Two steps correspond to either zero or one atom in the trap. (c) Experimental time sequence for dephasing investigation. We depict the MOT magnetic field, compensatory and quantization magnetic fields as B_{MOT}, B_{com} and B_{quan}, respectively. See text for details.

Our experimental setup is depicted in Fig. 1(a) and has been described in detail elsewhere [30]. Formed by six counter-propagating cooling lasers (I_{cool}, where I is the intensity of the beam and an overlap repumping laser (I_{rep}), the magneto-optical trap (MOT) is loaded from background rubidium atoms in ultrahigh vacuum chamber. A laser beam propagating along z-axis with 830 nm wavelength (I_{dip}) is tightly focused in the center of the MOT by a commercial microscopic objective (N.A. = 0.38). The resulting far-off-resonance trap (FORT) has a waist of 2.1 μm. Its potential depth is 0.7 mK for a laser power of 7 mW. By reducing the intensity and increasing the detuning of the MOT cooling beams, single atoms can be localized in the FORT

#200990 - $15.00 USD Received 7 Nov 2013; revised 5 Dec 2013; accepted 9 Dec 2013; published 18 Dec 2013

based on “collisional blockade ”mechanism [31]. This trap provides the storage time of about ten seconds in the absence of any near-resonant light. The lifetime is limited by collisions with background gas and the heating mechanisms due to intensity fluctuations and photon scattering of the trap laser. Measured by a release-and-recapture technique, the temperature of single atoms is about 40 μK. This value ensures that the mean kinetic energy of trapped atoms is much smaller than the potential depth. Therefore, the optical potential can be approximated by a harmonic oscillator, and the calculated axial and radial oscillation frequencies are $2\pi \times 3.5$ kHz and $2\pi \times 39.2$ kHz. The laser induced fluorescence of single atoms is collected with the same objective, then coupled into a fiber and guided to an avalanche photodiode (APD) assembled in a single photon counting module. Shown in Fig. 1(b), the fluorescence signals allow us to discriminate whether one atom is trapped or not.

Single atoms can be prepared in $|F=2\rangle$ or $|F=1\rangle$ using the MOT laser beams. We define the logical states as $|1\rangle \equiv |F=2, m_F=0\rangle$ and $|0\rangle \equiv |F=1, m_F=0\rangle$. The quantization axis is generated by a bias magnetic field of $B=3$ G along z-axis. To compensate for the background magnetic field, three orthogonal pairs of coils are applied. The qubit is initialized in the state $|1\rangle$ by optically pumping. For this a π-polarized laser beam (I_{pum}) propagates along x-axis resonant with the $|F=2\rangle \rightarrow |F'=2\rangle$ transition. Single qubit rotations between states $|0\rangle$ and $|1\rangle$ are performed by two-photon stimulated Raman transition. The Raman laser beams ($I_{\text{R1}}, I_{\text{R2}}$) are formed by the $\pm 1^{\text{st}}$ orders diffraction of a 3.4 GHz acoustic-optical modulator (AOM). The zeroth order diffraction beam at 795 nm is red detuned 60 GHz from the D_1 transition. Both of the Raman beams are coupled into the same polarization maintaining optical fiber, and propagate along the quantization axis with circular polarization. They are focused in the chamber and overlapped with single atoms. The total power is 30 μW. For the state-selective detection, a circularly polarized probe laser beam (I_{prob}) resonant with the $|F=2\rangle \rightarrow |F'=3\rangle$ transition is applied to push out single atoms in the state $|F=2\rangle$. However, atoms in the state $|F=1\rangle$ are not influenced by this laser and remain in the trap. The internal states are therefore mapped onto the presence of atoms.

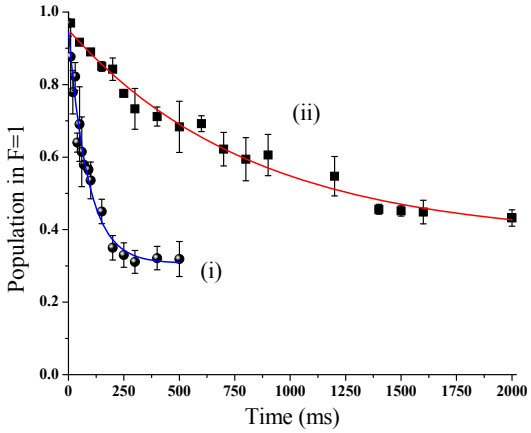

Fig. 2. Measurement of spin relaxation time. Single atoms is initialized in the state $|F=1\rangle$. After a variable trapping time, the push-out technique is applied to determine the atomic state. The fraction in $|F=1\rangle$ is recorded as a function of the trapping time. Each data is averaged over 200 single atoms. (i) Due to incoherent transitions induced by the background light of the dipole trap laser, the spin relaxation time is $T_1 = 0.087 \pm 0.009$ s. (ii) With an interference filter to reduce the background, the obtained time is $T_1 = 0.83 \pm 0.11$ s.

#200990 - $15.00 USD Received 7 Nov 2013; revised 5 Dec 2013; accepted 9 Dec 2013; published 18 Dec 2013

3.2. *Spin relaxation measurement*

In order to measure the spin relaxation time, we switch off the MOT laser beams in proper sequence and prepare single atoms in the state $|F=1\rangle$. After a variable trapping time, the push-out laser beam is applied. We switch on the MOT beams again to determine whether the atom is still present. The fraction of single atoms in $|F=1\rangle$ is recorded as a function of the trapping time, as shown in Fig. 2. Each data is averaged over 200 single atoms.

In our experiment, the optical dipole trap at 830 nm wavelength is from an external cavity diode laser. It has a broad spectrum background light, including photons resonant with the rubidium D_1 and D_2 transitions. Due to incoherent transitions induced by the background, the obtained spin relaxation time is only $T_1 = 0.087 \pm 0.009$ s. To eliminate this influence, we insert a narrow band interference filter (Semrock FF01-830/2-25) with central transmitting wavelength 830 nm. It has a full width at half maximum (FWHM) of 10.4 nm and a peak transmission of 95%. The optical densities of 780 nm and 795 nm are close to 7. As a consquence, we almost completely remove the resonant photons from the optical dipole trap. The measurement spin relaxation time reaches $T_1 = 0.83 \pm 0.11$ s. To compare with theory, we calculate the relaxation rate of the hyperfine-level populations using the Kramers-Heisenberg formula [13]. Under our conditions, the theoretical spin relaxation time is 0.91 s. The improved good agreement between theory and experiment is noted.

3.3. *Phase decoherence suppression*

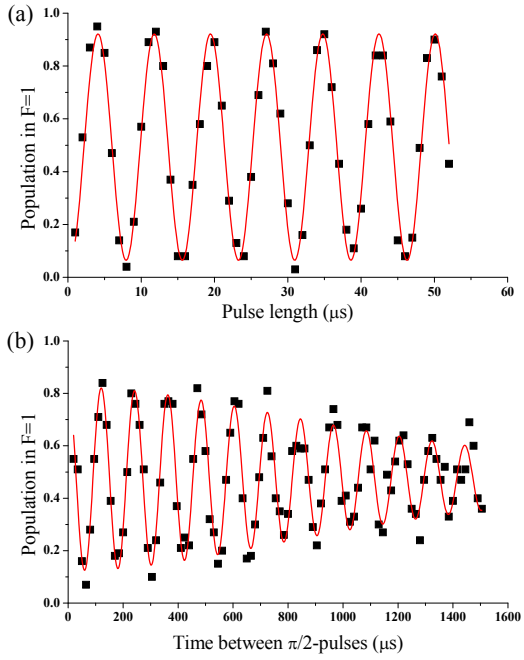

Fig. 3. (a) Rabi oscillations between $|F=1, m_F=0\rangle$ and $|F=2, m_F=0\rangle$ states. The fraction of single atoms in the state $F=1$ is measured as a function of Raman pulse length. We observe a sinusoidal variation with high contrast. The Rabi frequency is $\Omega_R = 2\pi \times$ 130 kHz. This value corresponds to a $\pi/2$ rotation time of 1.9 μs. (b) Ramsey spectroscopy recorded with a fixed two-photon detuning from the ground-state hyperfine splitting. The detuning is $\delta = 2\pi \times 8.6$ kHz. We fit the fringes according to the model presented in [14]. The measured dephasing time is $T_2^* = 1.4 \pm 0.1$ ms.

#200990 - $15.00 USD Received 7 Nov 2013; revised 5 Dec 2013; accepted 9 Dec 2013; published 18 Dec 2013

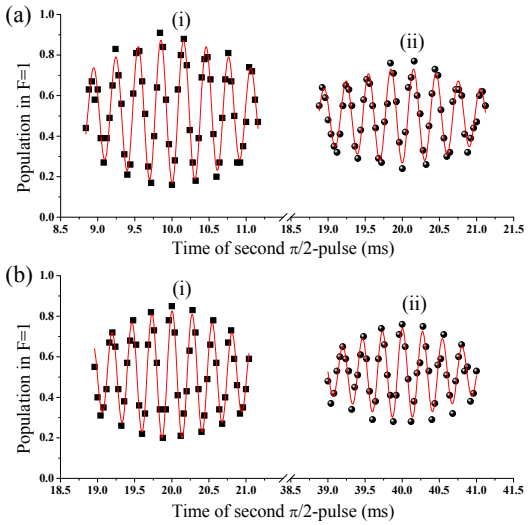

Fig. 4. Examples of the spin echo and CPMG signals. We plot fringes as a function of the time of second $\pi/2$-pulse. (a) For spin echo method, the time of π-pulse is fixed to be $\tau = 5.0$ ms (i), 10.0 ms (ii). (b) For CPMG sequence with $n = 2$, the first π-pulse is applied at time $\tau = 5.0$ ms (i), 10.0 ms (ii), and thus the second $\pi/2$-pulse is at time $t = 4\tau$. These graphs are fitted using the model in [14] and in the text. The initial visibility decreases with increasing time τ.

The experimental time sequence for dephasing investigation is shown in Fig. 1(c). Once single atoms are trapped, we shut off the MOT laser beams and magnetic field (depicted as B_{MOT}), meanwhile turn on the compensatory and quantization magnetic field (depicted as B_{com} and B_{quan}, respectively). After a 50 ms interval to stabilize the magnetic fields, the qubit is initialized in state $|1\rangle$ using pumping and repumping laser beams. We then apply different Raman pulses to drive single qubit operation as desired, such as measuring dephasing time by Ramsey spectroscopy and suppressing dephasing via spin echo or CPMG pulses. At the end of the sequence, the MOT is switched on again, and the push-out technique allows us to determine the projection of the atomic state on any superposition. For each data point plotted in Figs. 3 and 4, we perform 100 cycles of this sequence.

Rabi oscillations on hyperfine levels of ground state are shown in Fig. 3(a). We vary the Raman pulse length from 1.0 μs to 52.0 μs in steps of 1.0 μs. A sinusoidal variation with high contrast is observed. Fitted with a sinusoidal, we obtain a two-photon Rabi frequency of $\Omega_{\mathrm{R}} = 2\pi \times 130$ kHz, which corresponds to a $\pi/2$ rotation time of 1.9 μs.

The dephasing time is measured by performing Ramsey spectroscopy. We apply two $\pi/2$-pulses with a fixed two-photon detuning δ separated by a variable time interval. During this time, atomic qubit evolves freely from a superposition of $|0\rangle$ and $|1\rangle$ states. As shown in Fig. 3(b), we observe the Ramsey fringes with detuning $\delta = 2\pi \times 8.6$ kHz. The decay of signal visibility as the free evolution time is due to the inhomogeneous dephaing. We fit the fringes using the model presented in [14] and obtain the inhomogeneous dephasing time of $T_2^* = 1.4 \pm 0.1$ ms.

This dephasing can be reversed by spin echo, which consists of an additional π-pulse at half of the free evolution time in the Ramsey process. Examples of spin echo signals are shown in Fig. 4(a) for different time between the first $\pi/2$-pulse and π-pulse, τ. These fringes are plotted as a function of the time of second $\pi/2$-pulse around $t = 2\tau$. Obviously, the inhomogeneous dephasing has been reversed. We refer to [14] and fit the spin echo signals. The visibility for

#200990 - $15.00 USD Received 7 Nov 2013; revised 5 Dec 2013; accepted 9 Dec 2013; published 18 Dec 2013

different time of spin echo is recorded in Fig. 5(a) and fitted with a Gaussian depicted in Eq. (10). The decrease of visibility results from the homogenous dephasing. Its corresponding phase decoherence time is $T_2' = 103 \pm 8$ ms (shown in Table 1).

During the spin echo process, the homogenous dephasing due to low frequency noise is suppressed partially. Nevertheless, in the presence of higher frequency noise, multipulse sequence is a better choice for more effectively suppressing as well as compensating the phase error of π-pulses [29]. In our experiment, we apply CPMG sequences with pulse numbers $n = 2, 3, 4, 5,$ and 6. The phase of π-pulse keeps the same as the value of $\pi/2$-pulse. Similarly to the spin echo signals, CPMG fringes are obtained by scanning the time of the second $\pi/2$-pulse. We fit the experimental data according to Eq. (7), as shown in Fig. 4(b). All the measured visibility signals are plotted in Figs. 5(b)–5(f) and fitted with a Gaussian depicted in Eq. (10).

The corresponding fit parameters are listed in Table 1. As shown in Fig. 6, the homogeneous dephasing time increases with number of CPMG pulses. For $n = 2$, the dephasing time is 133 ± 4 ms. For $n = 6$, the dephasing time is extended to 304 ± 17 ms. Once we increase pulse number $n > 6$, the fringe visibilities decrease significantly, mainly resulting from imperfections of π-pulses.

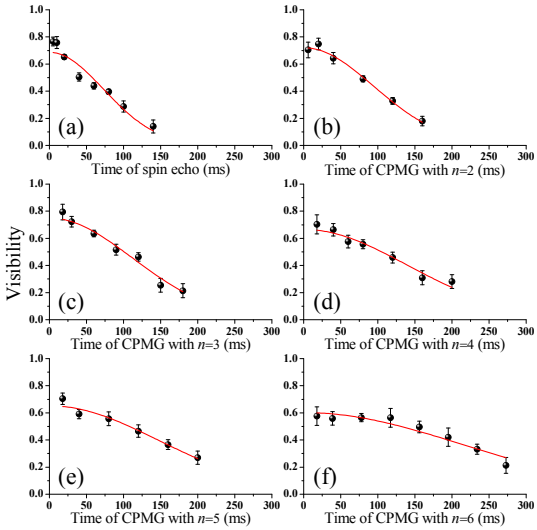

Fig. 5. Visibility of the spin echo and CPMG sequences as a function of the total time between two $\pi/2$-pulses. The values of spin echo (a) and CPMG sequences with pulse numbers $n = 2$ (b), 3 (c), 4 (d), 5 (e), and 6 (f) are extracted from the corresponding fringes similar to Fig. 4. We fit all the graphs with a Gaussian depicted in Eq. (10).

Table 1. Fit parameters extracted from the signals of spin echo and CPMG sequence of Fig. 5 using Eq. (10). The parameter n represents the number of π-pulses between two $\pi/2$-pulses. Spin echo is applied when $n = 1$.

	Fig. 5(a)	Fig. 5(b)	Fig. 5(c)	Fig. 5(d)	Fig. 5(e)	Fig. 5(f)
n	1	2	3	4	5	6
C_0 (%)	69±3	72±2	75±2	67±2	65±2	60±2
T_2' (ms)	103±8	133±4	159±8	197±11	209±13	304±17

#200990 - $15.00 USD Received 7 Nov 2013; revised 5 Dec 2013; accepted 9 Dec 2013; published 18 Dec 2013

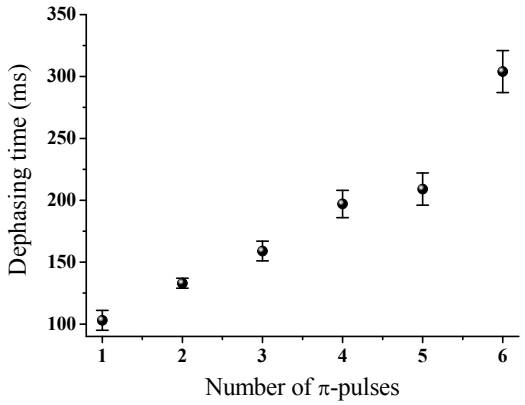

Fig. 6. Dephasing time as a function of number of π-pulses, n. Spin echo or CPMG sequences are applied when $n = 1$ or $n \geq 2$. The homogeneous dephasing time is extracted from the corresponding signals in Fig. 5. These data are shown in Table 1.

4. Discussions

Though the homogenous dephasing due to low frequency noise is suppressed partially in the spin echo process ($< 2/t, t = 2\tau$), CPMG pulse sequence performs better for higher frequency noise ($< 2n/t, t = 2n\tau$). In the field of trapped neutral atoms, it was in an atomic ensemble that CPMG pulse sequence was studied before our work. For atomic ensembles, collisions between trapped atoms can increase higher frequency components. Therefore, the effect of suppressing dephasing is efficient when a plenty of π-pulses are applied, especially in a dense ensemble. Via CPMG sequence with 10 π-pulses, the coherence time reached a 2.5-fold improvement as compared to the value in the spin echo process [22]. Later in an ensemble at high density, utilizing the CPMG sequence with more than 200 π-pulses, a 20-fold increase of coherence time was demonstrated in [23]. In our work, as frequency noise due to atomic collisions disappears for single atoms, the homogenous dephasing is mainly induced by laser intensity and beam pointing instabilities, magnetic field fluctuations. As a consequence, CPMG suppression effect could be clearly observed with only a few π-pulses. For our trap $U_0 = 0.7$ mK, the homogeneous dephasing time is already prolonged by a factor of 3 via CPMG sequence with $n = 6$. It reaches $T_2' = 304 \pm 17$ ms. By contrast, in the previous experiments without CPMG sequence, the measurement dephasing time of single atoms was significantly short. For $U_0 = 1.2$ mK, Grangier's group obtained the dephasing times of $T_2^* = 0.37$ ms and $T_2' = 13$ ms in the spin echo process [27]. The dephasing time of $T_2^* = 0.87$ ms for $U_0 = 1.0$ mK was reported by Saffman's group [32]. In order to obtain longer coherence time, we will investigate the fluctuations of noise spectra in detail and optimize dynamical decoupling [33].

The inhomogeneous dephasing is successfully reversed via spin echo and CPMG pulse sequence. However, its corresponding time remains $T_2^* = 1.4 \pm 0.1$ ms. This results from unchanged atomic energy distribution. We can reduce inhomogeneous broadening utilizing the adiabatic lowering of the trap depth and Raman sideband cooling techniques. Under our experimental conditions, the obtained spin relaxation time is $T_1 = 0.83 \pm 0.11$ s. This measured time is consistent with the calculated value. For quantum information processing, fundamentally $T_2 \leq 2T_1$ [2]. If longer dephasing time is expected, we have to further suppress the spin relaxation of atoms. An optical dipole trap with larger detuning and smaller depth can be used. Meanwhile, it is worth considering suppressing both transverse relaxation and longitudinal relaxation

#200990 - $15.00 USD Received 7 Nov 2013; revised 5 Dec 2013; accepted 9 Dec 2013; published 18 Dec 2013

via some multipulse sequences, such as the CDD, concatenation of the UDD sequence (CUDD) and quadratic UDD (QDD) [33]. Moreover, in comparison with the red-detuned trap, photon scattering and motional decoherence effects are significantly reduced in the blue-detuned trap [34]. The coherence time $T_2^* = 43$ ms of single cesium atoms was observed in a 532 nm wavelength bottle beam trap [35]. The suppression effect of multipulse sequence for single atoms in the dark trap is anticipated.

5. Conclusions

In conclusion, we have performed CPMG sequence with different pulse numbers in single Rb atom experiments and demonstrated the strong suppression of dephasing. We analyzed the effect of CPMG sequence and experimentally confirmed that it could efficiently suppress both inhomogeneous and homogeneous dephasing mechanisms for single neutral atoms. We believe this method will be useful in further experiments of quantum information processing and precision measurements with single neutral atoms.

Acknowledgments

This work was supported by the National Basic Research Program of China under Grant No.2012CB922101, the National Natural Science Foundation of China under Grant Nos.11104320 and 11104321, and funds from the Chinese Academy of Sciences.

#200990 - $15.00 USD Received 7 Nov 2013; revised 5 Dec 2013; accepted 9 Dec 2013; published 18 Dec 2013